AD-A136 217 ROTORDYNAMIC FORCES DEVELOPED BY LABYRINTH SEALS(U) 1/1
TEXAS A AND M UNIV COLLEGE STATION TURBOMACHINERY LABS
D W CHILDS ET AL. OCT 83 AFOSR-TR-83-1133
UNCLASSIFIED F49620-82-K-0083 F/G 20/4 NL

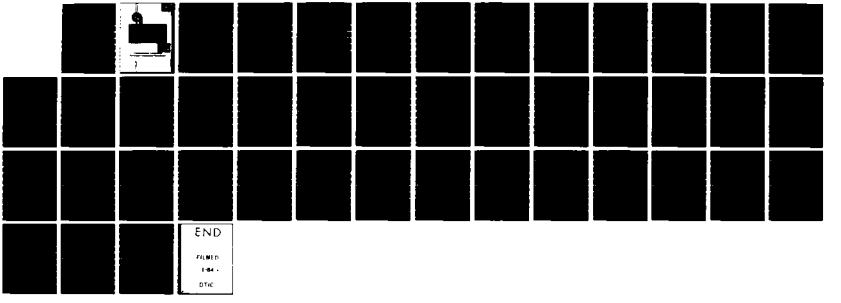

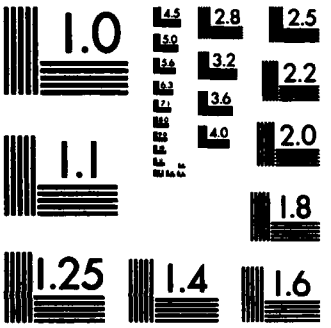

MICROCOPY RESOLUTION TEST CHART
NATIONAL BUREAU OF STANDARDS-1963-A

ROTORDYNAMIC FORCES DEVELOPED BY LABYRINTH SEALS

BY

DARA W. CHILDS

DAVID L. RHODE

SECURITY CLASSIFICATION OF THIS PAGE (When Data Entered)

REPORT DOCUMENTATION PAGE	READ INSTRUCTIONS BEFORE COMPLETING FORM
1. REPORT NUMBER: AFOSR-TR- 83-1133	2. GOVT ACCESSION NO.: AD-A136 217
	3. RECIPIENT'S CATALOG NUMBER:
4. TITLE (and Subtitle): ROTORDYNAMIC FORCES DEVELOPED BY LABYRINTH SEALS	5. TYPE OF REPORT & PERIOD COVERED: ANNUAL 1 SEPT 82 - 31 AUG 83
	6. PERFORMING ORG. REPORT NUMBER:
7. AUTHOR(s): DARA W CHILDS; DAVID L RHODE	8. CONTRACT OR GRANT NUMBER(s): F49620-82-K0083
9. PERFORMING ORGANIZATION NAME AND ADDRESS: TEXAS A&M UNIVERSITY; COLLEGE STATION, TEXAS 77843-3123	10. PROGRAM ELEMENT, PROJECT, TASK AREA & WORK UNIT NUMBERS: 61102F 2307/B1
11. CONTROLLING OFFICE NAME AND ADDRESS: AIR FORCE OFFICE OF SCIENTIFIC RESEARCH /NA; BOLLING AIR FORCE BASE, D.C. 20332	12. REPORT DATE: OCTOBER 1983
	13. NUMBER OF PAGES: 39
14. MONITORING AGENCY NAME & ADDRESS(if different from Controlling Office)	15. SECURITY CLASS. (of this report): UNCLASSIFIED
	15a. DECLASSIFICATION/DOWNGRADING SCHEDULE

16. DISTRIBUTION STATEMENT (of this Report)

Approved for public release; distribution unlimited.

17. DISTRIBUTION STATEMENT (of the abstract entered in Block 20, if different from Report)

18. SUPPLEMENTARY NOTES

19. KEY WORDS (Continue on reverse side if necessary and identify by block number)
LABYRINTH SEAL
ROTORDYNAMIC FORCES
NUMERICAL ANALYSIS

20. ABSTRACT (Continue on reverse side if necessary and identify by block number)

Numerous tasks have been completed in developing measurement and prediction techniques for accurately determining the fluid-structure-interaction forces on labyrinth seal rotors. The test facility has been designed, fabricated, and assembled; the drive mechanism and instrumentation system have been tested. Further, various improvements to the test apparatus have been implemented. Also, the development of two basic computational approaches for predicting seal rotor forces has been successfully completed. These consist of an improved but approximate analytical model and an extensive computer

DD FORM 1 JAN 73 1473 EDITION OF 1 NOV 65 IS OBSOLETE

UNCLASSIFIED

SECURITY CLASSIFICATION OF THIS PAGE (When Data Entered)

program incorporating the complete Reynolds-averaged Navier-Stokes equations. The latter model solves finite difference equations in predicting the two-dimensional (axisymmetric) compressible flow in a concentric-rotor labyrinth seal cavity. Details of a corresponding incompressible flow prediction are presented and discussed. The final numerical model will allow prediction of the desired three-dimensional, eccentric-rotor flow field and the associated rotordynamic forces.

TABLE OF CONTENTS

I. Introduction

Seals develop fluid-structure-interaction forces due to the relative motion of the rotor and housing at seal locations, and these forces have been shown to have a significant influence on the rotordynamic stability and response characteristics of high performance turbomachinery. The present research effort was initiated in September of 1982, and is a combined computational-experimental program to develop experimentally-validated computational approaches for predicting seal forces. More specifically, computational approaches are being developed to define the force coefficients for the force-motion relationship:

$$-\begin{Bmatrix} F_X \\ F_Y \end{Bmatrix} = \begin{bmatrix} K & k \\ -k & K \end{bmatrix} \begin{Bmatrix} X \\ Y \end{Bmatrix} + \begin{bmatrix} C & c \\ -c & C \end{bmatrix} \begin{Bmatrix} \dot{X} \\ \dot{Y} \end{Bmatrix} \qquad (1)$$

where (X,Y) are components of the relative displacement vector between the rotor and the stator at the seal location, and (F_X, F_Y) are components of the reaction force resulting from transient pressure and velocity distributions within the seal. The computational approaches which are being developed in this study will define the pressure and velocity distributions within the seal which result from relative rotor-stator motion. The computational approaches are to be validated by comparison to experimental measurements of the following quantities:

(a) transient pressure measurements at the seal-stator wall ,

(b) transient measurements of the displacement (X,Y) and

force (F_X,F_Y) components, which results in calculated values for the rotordynamic (stiffness and damping) coefficients of Eq. (1), and

(c) laser velocimeter measurements of the velocity distributions within labyrinth seal cavities.

Dr. Childs and Dr. Rhode are responsible, respectively, for the experimental and computational developments. In the following two chapters, reviews are provided of the research accomplishments with respect to these two complementary facets of the research project.

II. Experimental Developments

A. Introduction

The experimental developments of this program are jointly supported by NASA and AFOSR. NASA funds ($223,749; 1 June 1981 to 13 December 1983) have been used to develop the test facility and test apparatus and to support analytical-computational developments. NASA officials are primarily interested in annular seals having constant-clearance or convergent-taper geometries with smooth and honeycomb stator surfaces. Their interest in this type of seal arises from applications in the turbine areas of the high-pressure turbopumps of the Space Shuttle Main Engine. This status report reviews the experimental progress of the complete program without distinguishing between sources of support.

B. Test Apparatus

The test apparatus was designed and its manufacture was supervised by Dr. John Dressman of the University of Louisville who served as a subcontractor. It was delivered to TAMU in January 1983, and has since been modified in the following respects:

(a) The housing has been modified to accept "swirl-rings" at the inlet. These swirl-rings are provided to pre-rotate the entering fluid in the circumferential direction. The fluid may be rotated in either the same direction or the opposite direction of rotation for the seal rotor. Alternatively, straightening vanes are provided to minimize fluid prerotation. Prior test results have shown that the inlet tangential velocity is a critical factor in defining the "stiffness-cross-coupling" coefficient k of Eq. (1).

(b) The housing has been modified to provide access for additional pressure instrumentation at the seal. This instrumentation includes both an inlet pitot tube and pressure taps along the seal.

(c) The test rotor has been modified to accept two couplings which will allow it to be driven by either an electric motor (to 5300 rpm) or by an air turbine (to 20,000 rpm).

(d) An additional port has been machined in the housing for access by the LDA system.

(e) Additional holes have been provided in the housing to provide access to the stator for mounting accelerometers.

(f) A new stator has been manufactured with static pressure taps along the seal and an inlet pitot-tube measurement for inlet tangential-velocity measurement.

(g) A new high-speed rotor has been manufactured which can run out to 20,000 rpm.

The test apparatus utilizes an external shaker to excite the rotating seal within its stator. The shaker was purchased using AFOSR funds ($29,000) and has been received and checked out. Some problems were encountered at the outset; however, the unit's manufacturer (Zonic Corporation) has resolved the problem satisfactorily.

All auxiliary instrumentation, drive-motors, bearing-lube systems, etc., have been purchased and checked out.

C. Test Facility

The test facility uses an Ingersoll-Rand screw compressor (1200 SCFM @ 100 psi) to supply air to the seal-test apparatus and a Sullair screw compressor (600 SCFM @ 120 psi) to an air turbine which has the capacity to rotate the seal up to 20,000 rpm. The compressors were purchased by TAMU using state funds and industrial contributions. Both the compressors and the connecting piping to the test section have been installed. All of the requisite instrumentations, controls for the flow circuit, plumbing, electrical wiring, controls, etc., have been purchased, installed, and checked out. Pending some future unpleasant surprise, which would necessitate additional work, the test facility is now completed.

D. Graduate Student Development

Mr. Joseph Scharrer has been working on this project since 1 January 1983. Mr. Scharrer concluded his B.S. degree in Mechanical Engineering at Northern Arizona University in May of 1981 (in three years). He has been accepted into the AFRAPT program by TAMU and General Electric at Lynn, Massachusetts. Mr. Scharrer has been responsible for a great deal of the experimental development work on this project, and has recently developed an improved prediction model for rotordynamic-coefficients of a labyrinth seal. Mr. Scharrer's developments have extended Iwatsubo's analysis [1] to choked flow conditions, and incorporated a significantly improved leakage analysis in the solution procedure. The analysis developed by Scharrer is much cruder than that being developed under Dr. Rhode's direction. However, it is also much simpler and provides an interim prediction tool for comparison to experimental test results.

E. Summary

During the past year, development of the experimental facility was completed, while improvements and various modifications to the test apparatus were implemented. An improved but approximate analytical solution has been developed for the prediction of rotordynamic coefficients of labyrinth seals.

III. Computational Developments

The serious need for a complete recirculating flow model for compressible flow labyrinth seals was highlighted at a recent

workshop [2] held at TAMU regarding rotordynamic instability problems. Development of a user-simplistic, experimentally-validated, finite difference computer code has begun for predicting the pressure and velocity fields and subsequently the four rotordynamic force coefficients of Eq. (1).

The problem of subsonic air flow through a labyrinth seal is clearly elliptic, as recirculation zones have been observed in flow visualization experiments [3]. Also, it is three-dimensional because of rotor eccentricity effects which are of primary concern. It has been assumed that the rotor instability is manifested as a circular precessional orbit of frequency ω about the seal center position. The desired solution will be obtained from the steady-state form of the governing flow equations because a steady-state flowfield precesses along with the rotor in a r-θ plane.

Once the predicted pressure distribution (for a given orbital velocity ω) acting on the rotor is obtained, it will be employed to calculate the resulting F_r and F_θ forces. A second computation of the pressure and rotor force components at a different value of ω allows both the stiffness (K,k) and damping (C,c) coefficients to be calculated.

A. Literature Surveys

Substantial progress has been made toward the computation of rotordynamic labyrinth seal coefficients. First, several literature searches were conducted. The information sought was:
(a) near-wall velocity measurements near rotating surfaces to allow derivation of realistic wall functions needed for rotor surfaces,

(b) recent developments for reducing false diffusion, and (c) detailed velocity or pressure measurements within a labyrinth seal cavity. The overall findings of these searches was somehwat disappointing in that the state-of-the-art in the latter two areas is rather primitive. However, useful information has been obtained.

B. Computer Plotting

The second task completed constitutes the developme . . two computer software packages for plotting any of the quantities to be predicted with the finite difference code. Both of these graphics codes read labyrinth seal solution values from computer disk storage. One of these codes plots each of the desired radial profiles at the proper location (to scale) within the corresponding labyrinth seal outline enclosure. The second graphics package calculates the coordinates of contour lines (e.g., streamlines, isobars, etc.) and plots them at appropriate locations within the seal outline enclosure. At present, these graphics codes plot two-dimensional axisymmetric (i.e., concentric-rotor) predictions and are designed for easy extension to allow the option of plotting three-dimensional (eccentric-rotor) predictions as they become available. This plotting capability employs the GCS graphics package and is very helpful in developing the desired three-dimensional finite difference code.

C. Computer Code Development

Development of the required three-dimensional finite difference code for calculating rotordynamic force coefficients due to fluid

forces was undertaken in a logical, stepwise sequence of increasing complexity. The first task is essentially completed except for final prediction validation tests. This task consisted of developing a code for the two-dimensional (axisymmetric) compressible flow in a single cavity of a concentric-rotor labyrinth seal. This work largely consisted of extending a similar code previously developed by D. L. Rhode for incompressible flows in labyrinth seals, to allow the prediction of corresponding compressible flows.

The next section discusses the basic computational methodology and the development of the imcompressible flow code. The following two sections consider the extension for compressible flow and preliminary prediction results, respectively.

C.1 Incompressible Flow Model

The incompressible flow computer code for a labyrinth cavity was developed from an improved version of the advanced finite difference code recently developed by Lilley and Rhode [4]. The computational methodology employed is advantageous in that the task of extending it for three-dimensional flows is conceptually straightforward. Numerous modifications to this code were required in order to properly incorporate the labyrinth cavity boundary conditions and flow domain. These included a different approach for specifying the cavity inflow boundary values (discussed later) and the geometric and boundary condition complexities associated with the spinning surface. For example, it was decided that the code would have the capability of simulating cavity walls of arbitrary slope, as countless cavity configurations have been recently employed in the aerospace industry.

In the present model, all important physical mechanisms are simulated by the complete governing, elliptic, partial differential equations. These are the incompressible, axisymmetric form of the Reynolds-averaged equations for conservation of mass and momentum (with x,r,θ time-mean velocity components u,v,w) as well as appropriate turbulence transport equations required for the turbulence model. Each of these differential equations may be expressed in the general form

$$\frac{1}{r}\left[\frac{\partial}{\partial x}(\rho u r\,\phi)+\frac{\partial}{\partial r}(\rho v r\,\phi)-\frac{\partial}{\partial x}\left(r\Gamma_\phi\frac{\partial\phi}{\partial x}\right)-\frac{\partial}{\partial r}\left(r\Gamma_\phi\frac{\partial\phi}{\partial r}\right)\right]=S_\phi \qquad (2)$$

where ϕ represents any dependent variable (i.e., u,v,w,k, and ε), Γ_ϕ represents the appropriate diffusion flux coefficient, and the source S_ϕ contains any remaining terms. Symbols k and ε represent turbulence kinetic energy and turbulence energy dissipation rate. The various source terms for each equation have been recently presented by Lilley and Rhode and these are given in Table 1. The standard form of the k-ε turbulence model as described by Launder and Spalding [5] was employed to evaluate an assumed isotropic effective viscosity which is given by

$$\mu_{eff} = C_\mu \rho k^2/\varepsilon + \mu$$

The finite difference equations are solved using the well known SIMPLE approach [6] on a complex mesh illustrated in Fig. 1. The intersections, point P for example, of the solid lines mark the grid nodes where all variables except the u and v velocity components are stored. The latter are stored at points which are

denoted by arrows (and labeled w and s, respectively) located midway between the grid intersections, and the boomerang-shaped envelope encloses a triad of points with reference location P at (I,J). The different control volumes C, U and V which are appropriate for flow variables stored at the P, w and s locations, respectively, are given in Fig. 2.

The computational domain for a labyrinth cavity of interest is shown with a coarse mesh in Fig. 3. There are several methods of numerically simulating the wall portion which does not lie parallel to a grid line. In the interest of conceptual simplicity, the stairstep simulation approach as previously employed by Rhode, et al. [7] was utilized. In that study it was shown that, if one is careful, the error arising from this approximation is small in comparison to that of the turbulence model and of false diffusion.

The finite difference equations for each ϕ were obtained by integrating Eq. 2 over the appropriate control volume (centered about the location of ϕ) and expressing the result in terms of neighboring grid point values. The convection and diffusion terms became surface integrals of the convective and diffusive fluxes while the source term was linearized. This results in

$$[\rho u\phi - \Gamma_\phi \frac{\partial \phi}{\partial x}]_e A_e - [\rho u\phi - \Gamma_\phi \frac{\partial \phi}{\partial x}]_w A_w$$

$$+ [\rho v\phi - \Gamma_\phi \frac{\partial \phi}{\partial r}]_n A_n - [\rho v\phi - \Gamma_\phi \frac{\partial \phi}{\partial r}]_s A_s = [S_P \phi_P + S_U]\mathrm{Vol}$$

where subscripts n, s, e and w refer to north, south, east and west cell faces. The finite difference equation for each ϕ cell

became

$$a_P^{\phi}\phi_P = \sum_j a_j^{\phi}\phi_j + S_u^{\phi}$$

where

$$a_P^{\phi} = \sum_j a_j^{\phi} - S_P^{\phi}$$

and

$$\sum_j \equiv \text{sum over N, S, E and W neighbors}$$

Velocities u* and v* and pressure p* are only estimates prior to convergence and, for example, the axial momentum equation which is solved for u* is

$$a_P^u u_P^* = \sum_j a_j^u u_j^* + S_u + A_w(P_W^* - P_P^*)$$

The resulting local value of u* must be corrected in order to also be an approximate local solution of the mass conservation equation. This correction occurs via the pressure correction P' (calculated from mass and momentum conservation considerations) according to

$$u_p = u_p^* + D^u(P_W' - P_P')$$

where $D^u = A_w/a_P^u$. The radial velocity v is similarly corrected, whereas pressure is corrected by

$$P = P^* + P'$$

The P' equation is a type of Poisson pressure equation given by

$$a_P^P P_P' = \sum_j a_j^P P_j' + S_u^P$$

Numerical solution proceeds by iterating the following steps: (1) guess values of all variables; (2) calculate u* and v* from the momentum difference equations; (3) solve the pressure correction equation for P'; (4) obtain pressure P and corrected velocities u and v; (5) solve other difference equations for other ϕ variables successively; and (6) return to (2) using the new values as improved guesses.

The numerical scheme considers variables at points along a vertical grid line as unknowns (e.g., N, P, and S for each point P), whereas the latest values of each E and W neighbor are treated as known. The tridiagonal matrix algorithm (TDMA) is employed to sequentially solve the system of algebraic equations resulting for each vertical line, sweeping from left to right.

The boundary conditions were numerically incorporated via appropriate modification of the finite difference equation for computational cells adjacent to a boundary. Boundary values at the seal cavity flow inlet are naturally very important, but unfortunately remain unknown, as necessary quantitative flow measurements do not exist even at a single operating condition. Current plans here at Texas A&M University include extensive measurement of the necessary values using an advanced laser doppler anemometer. Due to this current lack of inlet boundary data, current practice is that for each iteration the inlet

values of each variable (except pressure) are assumed equal to the latest corresponding outlet values. This practice implies a series of geometrically identical cavities (with a non-stepped stator housing) and a streamwise periodic flow which occurs downstream of the first two or three cavities.

No boundary conditions are needed at the cavity outlet because of the upwind differencing formulation which occurs there for all variables. The x- and r-momentum equations require the zero convective and diffusive flux specification along walls which are normal to the respective velocity component directions. Boundary values for these two equations along walls which are parallel to respective velocity component directions are implied through the use of experimentally-based wall functions. Appropriate wall functions are similarly employed for the θ-momentum equation along all impervious walls. Wall functions are also used along wall boundaries for the k- and ε-equations as derived for swirling flows by Lilley and Rhode [4].

C.2 Compressible Flow Model

The incompressible flow code described above was extended to allow subsonic compressible flow computations in a labyrinth cavity. Four primary modifications were implemented to accomplish this. First, the fluid was assumed to be an ideal gas (air) and an expression for calculating density (the ideal gas law) was incorporated.

The second modification consisted of including another simultaneous partial differential equation (conservation of energy)

from which the temperature T would be determined. The energy equation in terms of stagnation enthalpy H is

$$\frac{\partial}{\partial x_i} (\rho v_i H) = \frac{\partial}{\partial x_j} (v_m \tau_{mj} + K \frac{\partial T}{\partial x_j})$$

where

$$H \equiv C_p T + \tfrac{1}{2} V^2$$

and the expression for τ_{mj} is given subsequently. This equation was expressed as

$$\frac{\partial}{\partial x_i} (\rho v_i H) = \frac{\partial}{\partial x_j} [v_m \tau_{mj} + \frac{K}{C_p} \frac{\partial}{\partial x_j} (H - \tfrac{1}{2} V^2)]$$

wherein C_p was assumed constant.

The general form of this equation which was incorporated is

$$\frac{\partial}{\partial x_i} (\rho v_i H) - \frac{\partial}{\partial x_j} (\Gamma_H \frac{\partial H}{\partial x_j}) = S_H$$

where

$$\Gamma_H = \frac{\mu}{Pr} = \frac{K}{C_p}$$

and

$$S_H = \frac{\partial}{\partial x_j} [v_m \tau_{mj} - \Gamma_H \frac{\partial}{\partial x_j} (\frac{V^2}{2})]$$

The enthalpy boundary conditions included the specification of inlet temperature values which must be known or estimated, and all walls were treated as adiabatic. Boundary conditions for the kinetic energy portion of H were specified through wall functions

as for the momentum equations.

The stres tensor τ_{ij} was augmented to account for compressibility effects in the usual way as the third modification. The resulting stress relation is given by

$$\tau_{ij} = \mu_{eff}(\partial v_i/\partial x_j + \partial v_j/\partial x_i) - \delta_{ij}\frac{2}{3}(\rho k + \underline{\mu_{eff}\ \partial v_m/\partial x_m})$$

where the underlined quantity is the new contribution, as it is not generally negligible for compressible flows. The alteration was effected where necessary, i.e., in the finite difference equations for u, v, k, ε and H.

The fourth modification involved the derivation and implementation of the compressible flow form of the equation for pressure correction P'; a literature search had revealed that this equation is not available. Some highlights of the derivation are briefly considered here for the simple case of one-dimensional axial flow. The derivation began with the discretized form of the steady flow mass conservation equation which is

$$(\rho u)_e - (\rho u)_w = 0 \qquad (3)$$

where the lower case subscripts refer to values at control volume faces.

A typical control volume for P' is centered at a typical P' storage location, i.e., a point labeled P in Figs. 1 and 2. It is the C control volume which is utilized for the P' equation. The east face mass flux, for example, was expressed as

$$(\rho u)_e = (\rho^*+\rho')_e \ (u^*+u')_e \approx \rho^*_e u^*_e + \rho^*_e u'_e + \rho'_e u^*_e$$

where the term $\rho'_e u'_e$ was neglected. It was assumed that

$$\rho'_e = \tfrac{1}{2}(\rho'_E+\rho'_P) = \tfrac{1}{2}(P'_E/RT_E + P'_P/RT_P)$$

using the ideal gas law (where capitalized subscripts refer to grid point values). From axial momentum considerations, one finds

$$u'_e = D^u_e \ (P'_P - P'_E)$$

and

$$u'_w = D^u_w \ (P'_W - P'_P)$$

where

$$D^u_e = A_e/a^u_p$$

and

$$D^u_w = A_w/a^u_p$$

as given earlier.

Upon substituting the appropriate east and west face mass flux expressions into Eq. (3), the following was obtained for the P' difference equation

$$[AE + AW + F] \ P'_P = AE \ P'_E + AW \ P'_W + \Delta\dot{m}^*$$

where

$$AE = (\rho_e^* D_e^u - u_e^*/2RT_E)$$

$$AW = (\rho_w^* D_w^u + u_w^*/2RT_W)$$

$$F = (u_e^*/2RT_E + u_e^*/2RT_P) - (u_w^*/2RT_W + u_w^*/2RT_P)$$

$$\Delta\dot{m}^* = \rho_w^* u_w^* - \rho_e^* u_e^*$$

The P' equation actually implemented was derived from the two-dimensional flow mass conservation equation, although the procedure exactly parallels that given here. The appropriate boundary condition which was implemented for this equation is P'=0 along all boundaries.

The predictive capability of the compressible flow code remains to be evaluated for a compressible labyrinth seal flow. This results from the lack of appropriate measurements for comparison. Measurements of well-documented similar flows are currently being sought for this purpose. However, a small sample of incompressible flow labyrinth seal measurements were found; these are employed in the next section in a preliminary prediction test case. The next section also includes detailed predicted results of another incompressible flow in a labyrinth seal, as these are of considerable interest.

D. Preliminary Predictions of the Concentric-Rotor Seal

D.1 Incompressible Flow Test Case

A computerized literature search indicated that only the paper by Stoff [8] gives detailed quantitative velocity measurements within a labyrinth seal cavity. Only the circumferential

mean velocity profile is presented; it was measured with a laser doppler anemometer at a single axial station located midway between adjacent teeth. These measurements were employed for preliminary verification testing of the current computer code, although much more data is needed for final testing. As previously mentioned, current plans are that G. L. Morrison will obtain the required measurements here using a laser doppler anemometer purchased with Defense Department funds.

Stoff utilized a large-scale model test section with identical (non-stepped) rectangular cavities through which water flowed. It is assumed that the flow conditions are characterized primarily by the axial and circumferential Reynolds numbers as well as the Taylor number. These are based on spatially averaged swirl velocity W, tooth-clearance average axial velocity U, kinematic viscosity ν, shaft radius r_{sh}, tooth clearance c, and radial distance from the shaft to the stator wall d;

$$Re_x = \frac{Uc}{\nu} \approx 1.7 \times 10^2$$

$$Re_\theta = \frac{Wd}{\nu} \approx 3.0 \times 10^4$$

$$T_a = \frac{Wd}{\nu} \left(\frac{d}{r_{sh}}\right)^{\frac{1}{2}} \approx 1.1 \times 10^4$$

Figure 4 shows that predictions using the incompressible flow computer code are in good agreement (6% discrepancy) with Stoff's corresponding measurements. Further, Stoff's computation employed the same numerical method and hybrid differencing scheme discussed

earlier and his predictions are essentially identical to those shown here.

D.2 Preliminary Predictions

The predicted results for the concentric-rotor case of an incompressible labyrinth seal flow field are included here. This serves to enhance one's understanding of the eccentric-rotor, compressible flow case which produces rotor instability forces. It is the "interstage" seal of the liquid hydrogen turbopump for the Space Shuttle main engine which is considered. Predictions were obtained for both a generic as well as a current seal design. Both of these designs exhibit a non-stepped stator wall. As noted earlier, this design feature alleviates the difficulty that the inlet flow boundary conditions are not known; i.e., it allows one to specify inlet values of each variable (except pressure) equal to corresponding outlet values for each numerical iteration. This results from the fact that the cavity inlet and outlet tooth clearance areas are the same. This practice assumes that the flow through a series of cavities is streamwise periodic.

All operating and geometrical conditions are typical of actual flight conditions. Liquid hydrogen at 42°R enters the cavity with tooth-clearance spatially averaged mean velocity U = 338 m/s. The primary dimensionless flow parameters (defined earlier) are: (a) $Re_x = 5.0 \times 10^5$, (b) $Re_\theta = 7.6 \times 10^5$, and (c) $Ta = 1.2 \times 10^5$. The shaft speed Ω = 35,410 rpm, cavity axial length $L = 8.585 \times 10^{-4}$m, and stator wall radius $R = 4.29 \times 10^{-2}$m.

A grid dependence study was conducted which revealed that a uniform 53 x 53 grid is satisfactory, exhibiting negligible grid

size effects. Convergence tests using convergence criteria as low as 0.05% for the normalized sum of residual mass source magnitudes, for example, were analyzed.

Figure 5 shows predicted dimensionless streamline patterns calculated and plotted by computer. The recirculation cell given in Fig. 5(a) is the expected result of a free shear layer flowing over a cavity. The predictions give no indication that an additional small recirculation cell exists in the corner at the base of each tooth. Note that for the case of negligible inlet (i.e., leakage) flow rate, a pair of counter-rotating Taylor-like cells are expected in the cavity. Stoff presents a predicted velocity vector plot of this case. Also, he shows a similar plot for the intermediate case of small inlet flow rate U/W = 0.06. This flow exhibits both recirculation cells, the upstream one being extended downstream near the free shear layer, and the other occupying only the lower right-hand corner of the rectangular cavity.

Also observe in Fig. 5(a) that the dividing streamline has a stagnation point slightly below the corner of the downstream tooth. This is also true of the typical cavity design as seen in Fig. 5(b). In the latter case the recirculation zone is centered slightly downstream and above that for the generic cavity. Also, the predicted recirculation strength is reduced to approximately 29% of the leakage flow rate, whereas it is 39% for the generic design.

As previously mentioned, many quantitative details for the flow field in a labyrinth cavity are not found elsewhere, particularly concerning the inlet boundary values. Therefore radial profiles of numerous flow variables are included here. Figure 6(a)

shows the dimensionless mean axial velocity distribution for the generic cavity. A very large value of $\partial u/\partial r$ occurs near the inlet separation corner; this is indicative of high turbulence energy generation in the free shear layer. The maximum velocity at a given axial station occurs very near the stator wall due to the large centrifugal force. The axial velocity distribution for the typical cavity in Fig. 6(b) is very similar. The most significant differences appear at $x/L = 0.35$ near the free shear layer and in the base of the cavity where the flow along the shaft is reduced.

As expected, there is negligible mean radial velocity in the leakage flow region as seen in Fig. 7(a), except near the stagnation point on the downstream tooth. This portion of the leakage flow is slightly increased for the typical cavity of Fig. 7(b). Seal designers can probably reduce this leakage contribution by altering the tooth shape at this location. The swirl velocity in Figs. 8(a) and (b) is normalized by the shaft circumferential velocity. The values for both seal designs are almost uniform throughout the entire domain, with a sharp increase very near a rotating surface.

Figures 9(a) and (b) show the distribution of pressure relative to the cavity inlet stator wall pressure P_{ow}. In the leakage flow region of the generic case, pressure decreases in the streamwise direction until about $x/L = 0.5$. Then it increases slightly until approximately $x/L = 0.78$, whereupon it suddenly decreases as the flow accelerates over the downstream tooth. This pressure variation is a reflection of the Bernoulli effect of pressure decrease at constrictions in flow area. These variations of flow area are

indicated by the dividing streamline in Fig. 5(a). Within the recirculation region also, pressure exhibits the expected behavior with the minimum value at the center of the vortex. A sharp positive pressure peak, which occurs in an annular fashion at $x/L = 0.85$, results from the flow stagnation on the downstream tooth. The resulting overall pressure drop from inlet to outlet of this cavity at the stated conditions is predicted as 600 kPa.

The pressure distribution within the typical cavity is seen if Fig. 9(b) to exhibit similar trends. However, leakage flow pressure varies in the streamwise direction much more gradually for this geometry, until about $x/L = 0.65$. Proceeding downstream, pressure decreases more rapidly than for the generic case as the flow area constricts in passing over the downstream tooth. Another effect of cavity design on pressure is the reduced level of $\partial P/\partial r$ within the typical cavity, a consequence of the reduced recirculation strength mentioned earlier. The predicted bulk pressure drop for this cavity is approximately an increase of 30% from the generic geometry. Thus, these pressure predictions reveal that the typical cavity is indeed preferred over the generic one.

As mentioned earlier, the large value of $\partial u/\partial r$ in the free shear layer yields a high generation rate of turbulence kinetic energy, which of course promotes the large overall pressure drop. Hence, the station maximum of turbulence energy occurs near the free shear region as seen in Figs. 10(a) and (b). Note that the typical cavity exhibits a significantly higher level of turbulence energy than for the generic case. The greatest value occurs in both cases at $x/L = 0.85$ near the stagnation point. A significant

portion of this turbulence energy is convected up and over the downstream tooth as indicated by the distribution at x/L = 1.0. The remainder is largely dissipated by viscous action in the recirculation zone.

The accuracy of the present predictions is difficult to assess due to the severe lack of suitable measurements for benchmark prediction tests of seal flows. The highly successful prediction of Stoff's swirl velocity measurements does, however, provide an indication of considerable realism. The present predictions do exhibit some degree of false diffusion (numerical) error, but this is largely limited only to the tip and base region of each tooth. An additional source of error for most swirling flow is inherent in the k-ε turbulence model, and thus, further work is needed in developing a more accurate approach to turbulence closure.

E. Summary

Progress in developing the necessary three-dimensional flow computer code for predicting the rotordynamic force coefficients included: (a) several computerized literature searches, (b) development of two graphics packages for computer plotting of predictions, (c) development of the task-one compressible seal flow prediction code, (d) preliminary prediction validation testing using Stoff's limited measurements, and (e) brief exploratory predictions to obtain additional insight regarding unknown seal flowfield boundary conditions, etc. The task-one code allows the prediction of the two-dimensional, axisymmetric air flow through a cavity of a concentric-rotor labyrinth seal.

Generation of this code involved numerous developments applied to an existing two-dimensional flow code. These included: (a) implementation of many computational domain boundary and boundary condition complexities, (b) incorporation of the conservation of energy differential equation, (c) addition of many stress terms resulting from compressibility effects, and (d) derivation and proper implementation of a new pressure correction equation.

F. Graduate Student Development

Mr. Steve Sobolik has been employed on this project since 1 September 1982. He received a B.S. degree (Cum Laude) in Mechanical Engineering from Texas A&M University in May 1982. He designed and developed software for Mitre Corp. (a NASA contractor) during three summers. Mr. Sobolik has been responsible for most of the computational development work on this project. He is an innovative individual and produces quality work.

G. Publications

A final manuscript concerning this investigation is currently in preparation as a technical journal article. Current plans are that it will be submitted to the ASME Journal of Fluids Engineering. The tentative title is: "On the Prediction of Incompressible Flow in Labyrinth Seals". Tentative authors include D. L. Rhode, S. R. Sobolik, and J. A. Demko.

H. Conference Presentations

The above paper has been accepted for presentation at the ASME Fluids Engineering Conference to be held in New Orleans, February 11 through 17, 1984. Also, an abstract entitled

"Prediction of Compressible Flow in a Labyrinth Seal" has been submitted to the Fluid Dynamics Division of the American Physical Society. The meeting will be held in Houston, November 20 through 22, 1983. Tentative authors are D. L. Rhode and S. R. Sobolik.

IV. References

1. Iwatsubo, T., Motouha, N., and Kawai, R., "Flow Induced Force of a Labyrinth Seal," NASA CP2250, Rotordynamic Instability Problems in High Performance Turbomachinery, Proceedings of a Workshop held at Texas A&M University, 10-12 May 1982.
2. "Workshop on Rotordynamic Instability Problems on High-Performance Turbomachinery," editors: D. Childs, R. Hendricks, J. Vance, Proceedings of a Workshop held at Texas A&M University, 12-14 May 1980, published as NASA CP2133.
3. Iwatsubo, T., "Evaluation of Instability Forces of Labyrinth Seals in Turbines or Compressors," NASA CP2133, Proceedings of a Workshop held at Texas A&M University entitled, "Rotordynamic Instability Problems on High-Performance Turbomachinery," 12-14 May 1980, pp. 139-167.
4. Lilley, D. G. and Rhode, D. L., "A Computer Code for Swirling Turbulent Axisymmetric Recirculating Flows in Practical Isothermal Combustor Geometries," NASA CR-3442, 1982.
5. Launder, B. E. and Spalding, D. B., "The Numerical Computation of Turbulent Flows," Comp. Methods in Appl. Mech. and Engr., Vol. 3, March 1974, pp. 269-289.

6. Gosman, A. D. and Pun, W. M., "Calculation of Recirculating Flows," Report No. HTS/74/2, 1974, Dept. of Mech. Engr., Imperial College, London.

7. Rhode, D. L., Lilley, D. G., and McLaughlin, D. K., "On the Prediction of Swirling Flowfields Found in Axisymmetric Combustor Geometries," ASME Jl. of Fluids Engr., Vol. 104, September 1982, pp. 378-384.

8. Stoff, H., "Incompressible Flow in a Labyrinth Seal," Jl. Fluid Mech., Vol. 100, 1980, pp. 817-829.

V. Tables

Table 1. The Form of the Source Term in the General Equation for ϕ (Eq. (2))

ϕ	S_ϕ
u	$-\frac{\partial p}{\partial x} + S^u$
v	$-\frac{\partial p}{\partial r} + \frac{\rho w^2}{r} - \frac{2\mu v}{r^2} + S^v$
w	$-\frac{\rho v w}{r} - \frac{w}{r^2}\frac{\partial}{\partial r}(r\mu)$
k	$G - C_D \rho \varepsilon$
ε	$(C_1 \varepsilon G - C_2 \rho \varepsilon^2)/k$

In this table certain quantities are defined as follows:

$$S^u = \frac{\partial}{\partial x}\left(\mu \frac{\partial u}{\partial x}\right) + \frac{1}{r}\frac{\partial}{\partial r}\left(r\mu \frac{\partial v}{\partial x}\right)$$

$$S^v = \frac{\partial}{\partial x}\left(\mu \frac{\partial u}{\partial r}\right) + \frac{1}{r}\frac{\partial}{\partial r}\left(r\mu \frac{\partial v}{\partial r}\right)$$

$$G = \mu\left[2\left\{\left(\frac{\partial u}{\partial x}\right)^2 + \left(\frac{\partial v}{\partial r}\right)^2 + \left(\frac{v}{r}\right)^2\right\} + \left(\frac{\partial u}{\partial r} + \frac{\partial v}{\partial x}\right)^2 + \left\{r\frac{\partial}{\partial r}\left(\frac{w}{r}\right)\right\}^2 + \left(\frac{\partial w}{\partial x}\right)^2\right]$$

VI. Figures

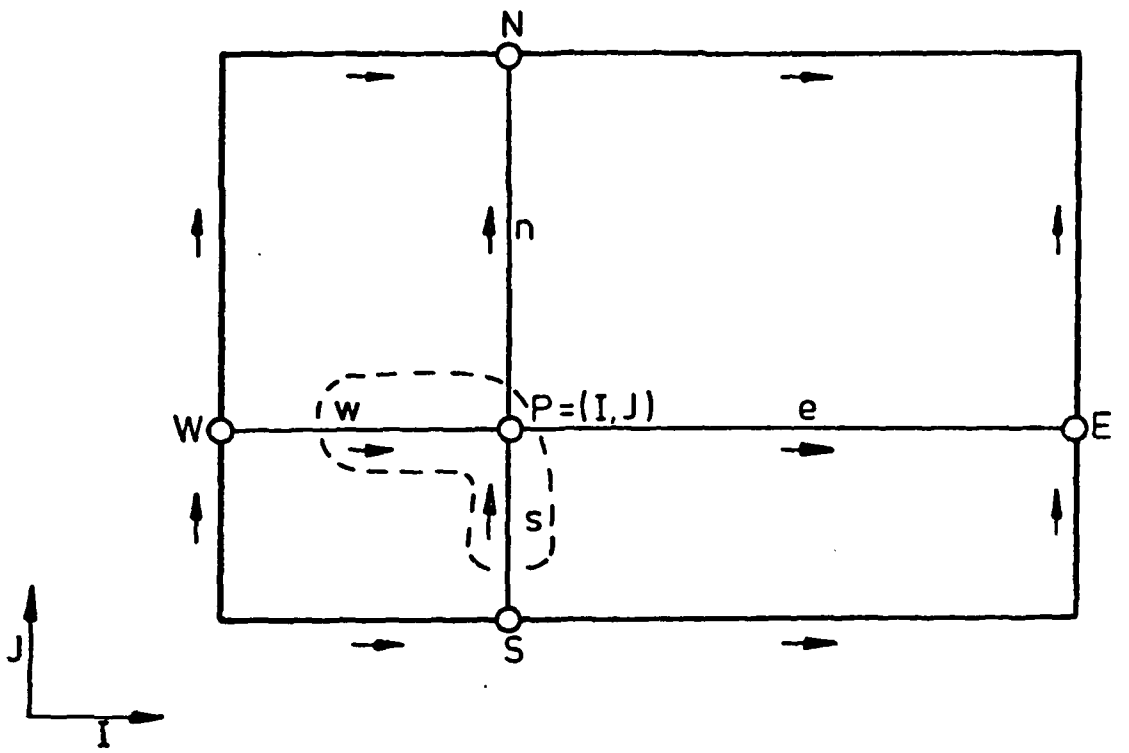

THREE GRIDS : FOR p, w ETC. - AT POSITION MARKED (O)
FOR u VELOCITY - AT POSITION MARKED (→)
FOR v VELOCITY - AT POSITION MARKED (↑)

Fig. 1. Staggered grid and notation for the rectangular computational mesh.

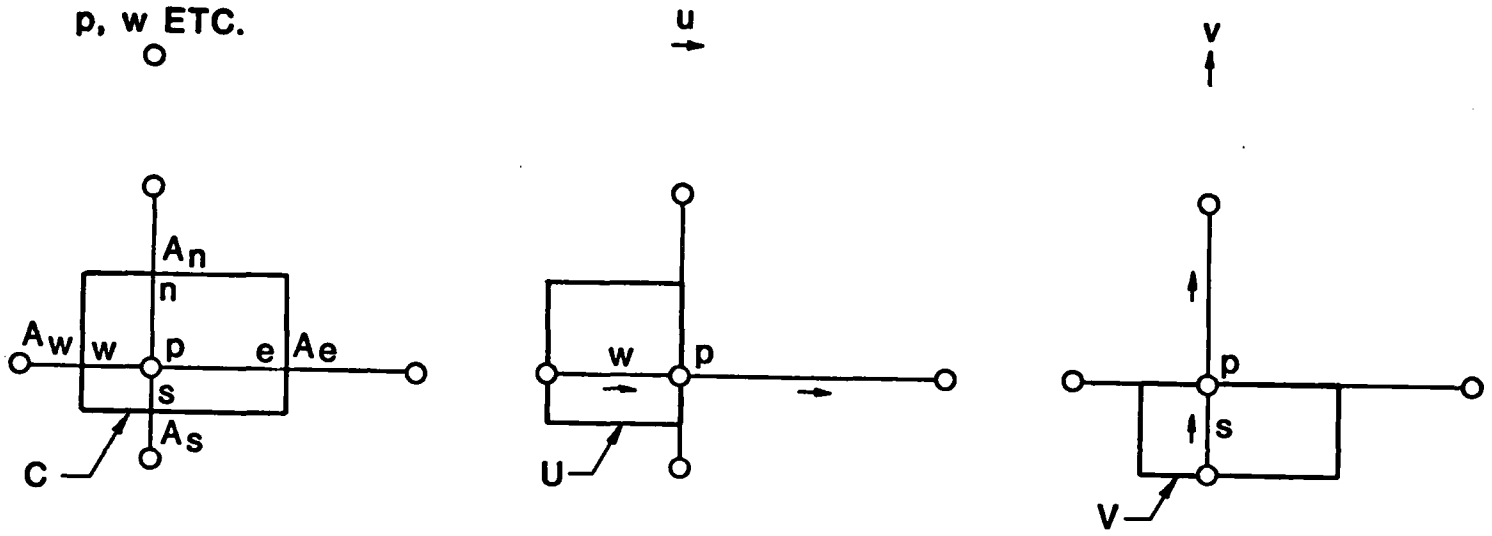

Fig. 2. The three control volumes associated with points of the three grids.

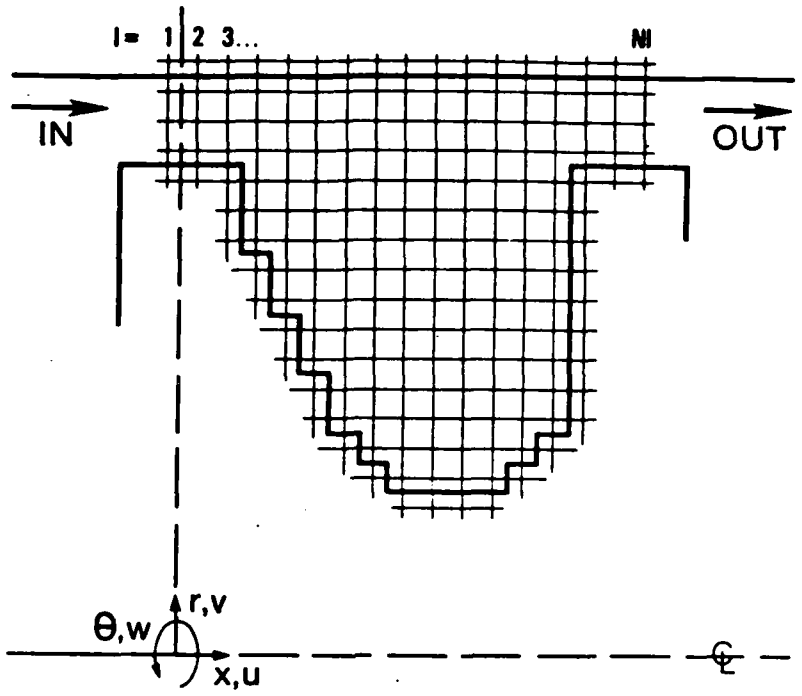

Fig. 3. Computational domain for a labyrinth seal cavity with a coarse grid

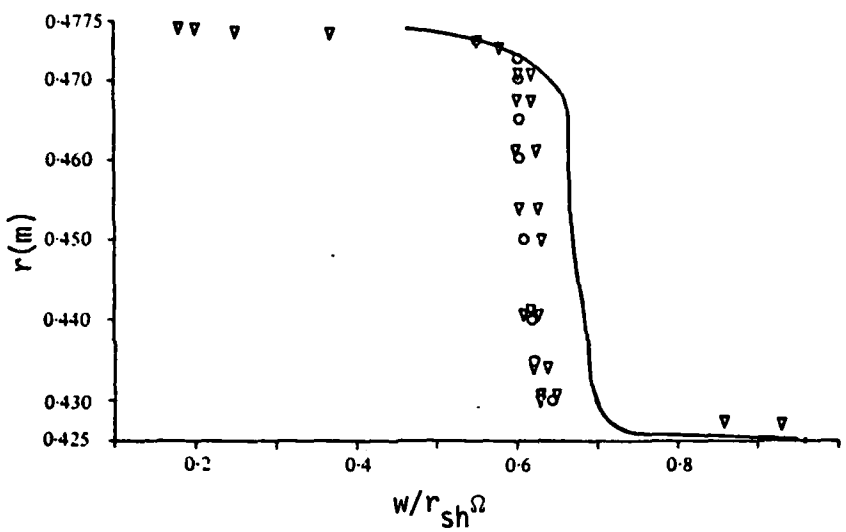

Fig. 4. Comparison of present predictions (————) of dimensionless swirl velocity with corresponding LDA measurements (o o o, ▽ ▽ ▽) of Stoff [8] at x/L = 0.5

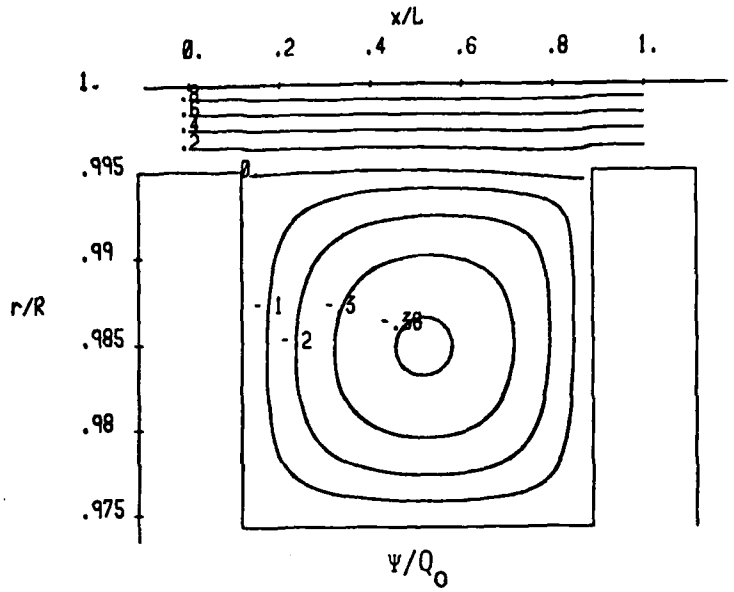

(a) Generic cavity

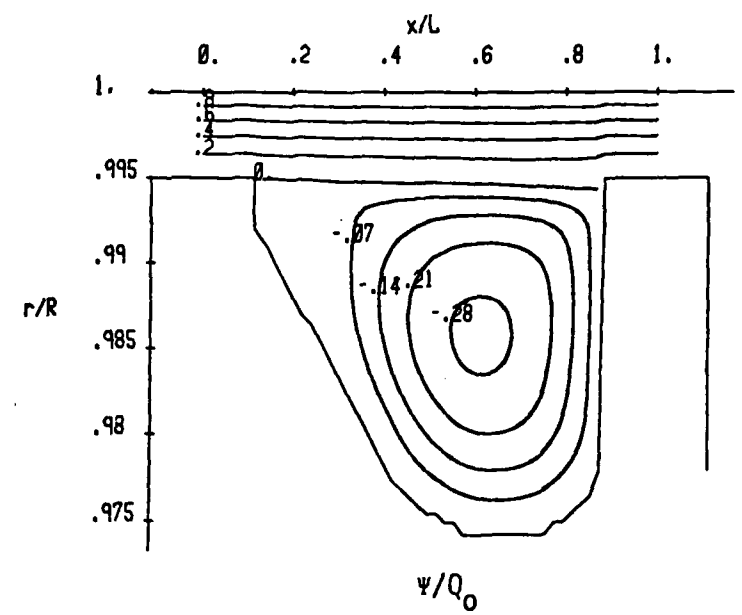

(b) Typical cavity

Fig. 5. Predicted dimensionless streamline pattern for: (a) a generic and (b) a typical labyrinth seal cavity

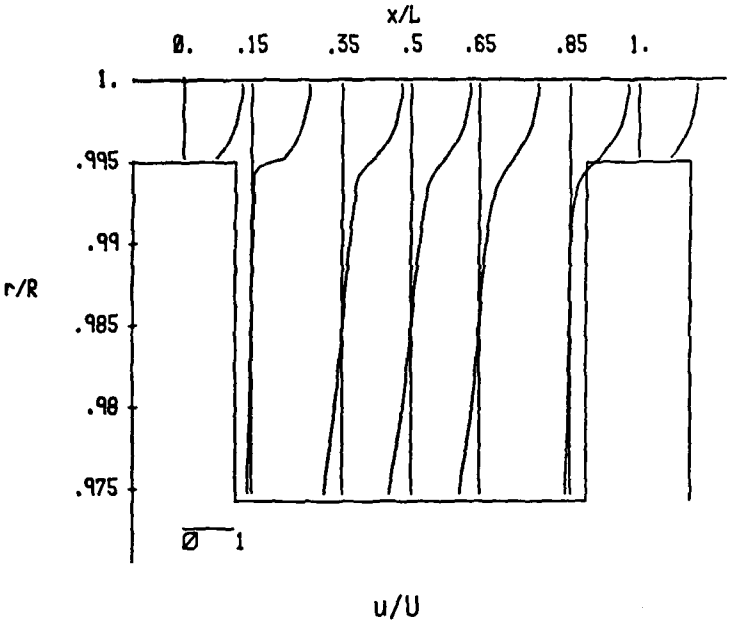

(a) Generic cavity

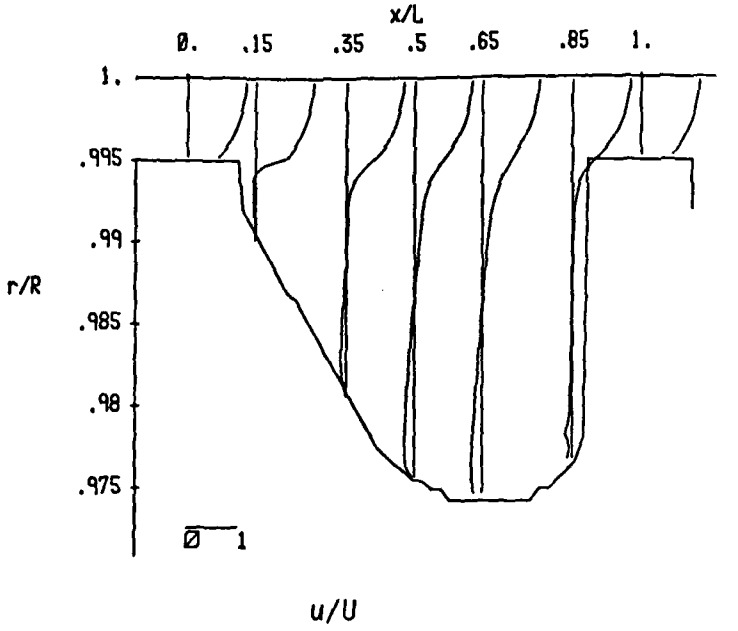

(b) Typical cavity

Fig. 6. Predicted dimensionless mean axial velocity for: (a) a generic and (b) a typical labyrinth seal cavity

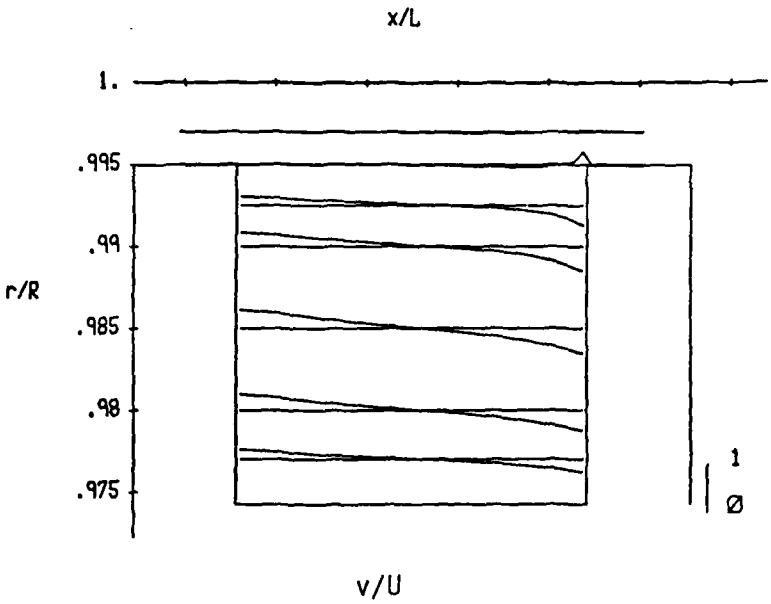

(a) Generic cavity

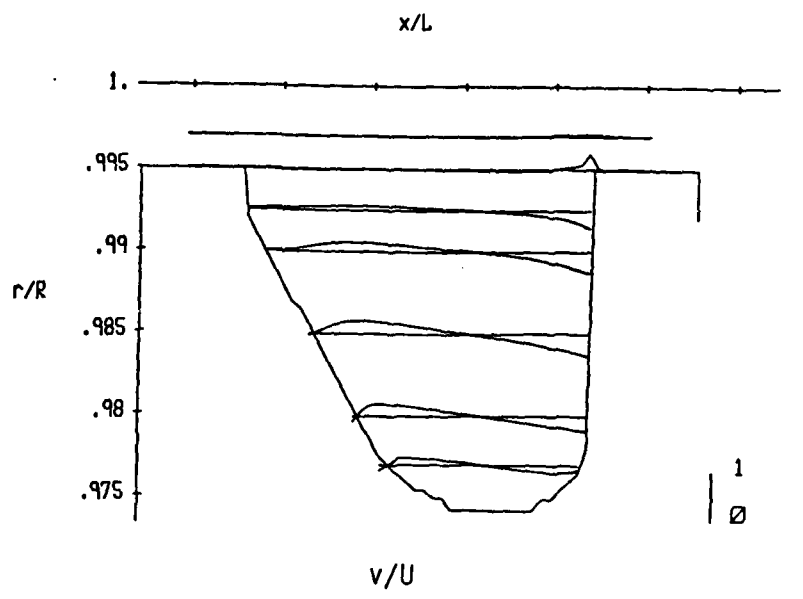

(b) Typical cavity

Fig. 7. Predicted dimensionless mean radial velocity for: (a) a generic and (b) a typical labyrinth seal cavity

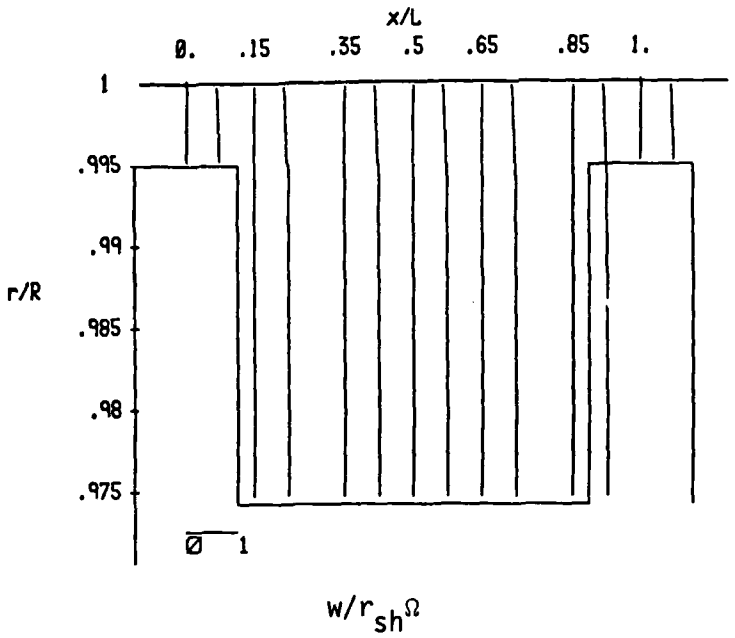

(a) Generic cavity

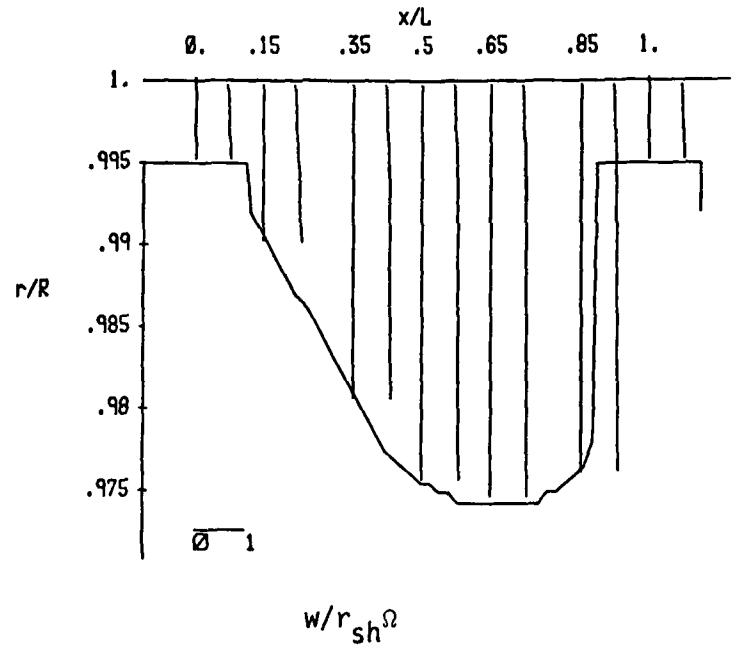

(b) Typical cavity

Fig. 8. Predicted dimensionless mean swirl velocity for: (a) a generic and (b) a typical labyrinth seal cavity

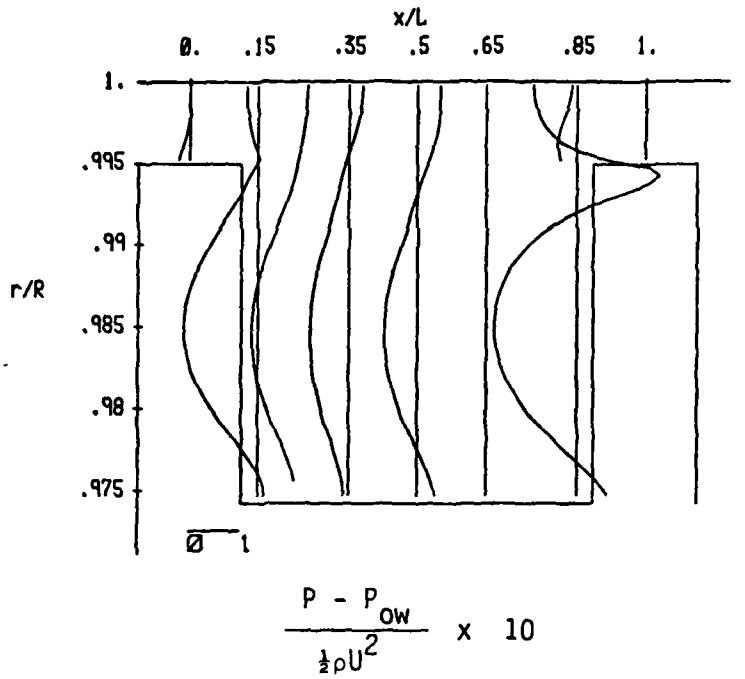

(a) Generic cavity

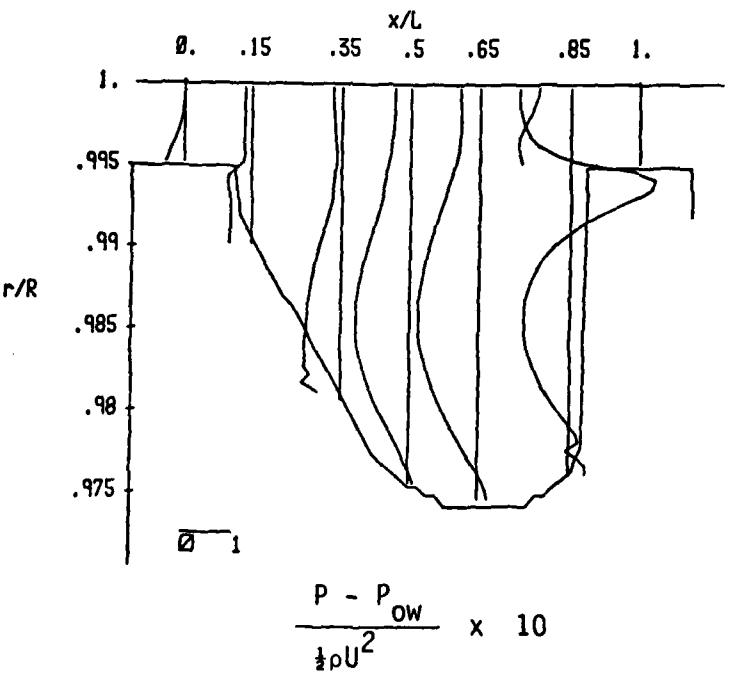

(b) Typical cavity

Fig. 9. Predicted dimensionless mean relative pressure for: (a) a generic and (b) a typical labyrinth seal cavity

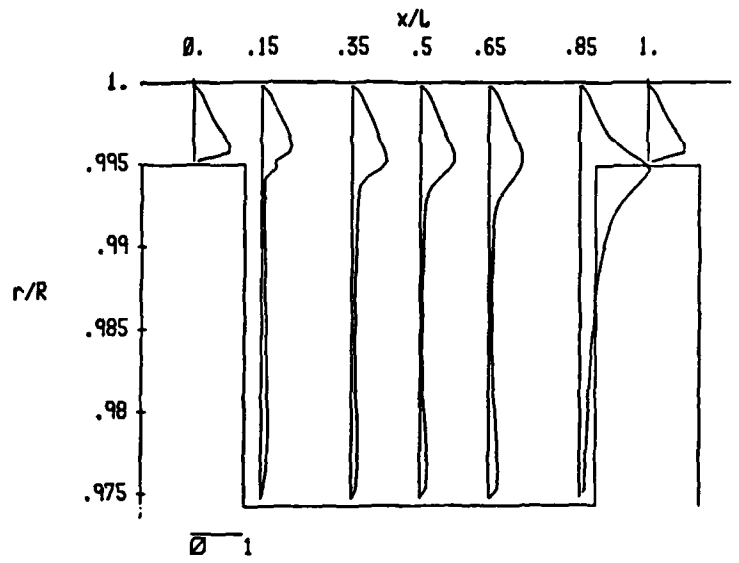

$k/U^2 \times 20$

(a) Generic cavity

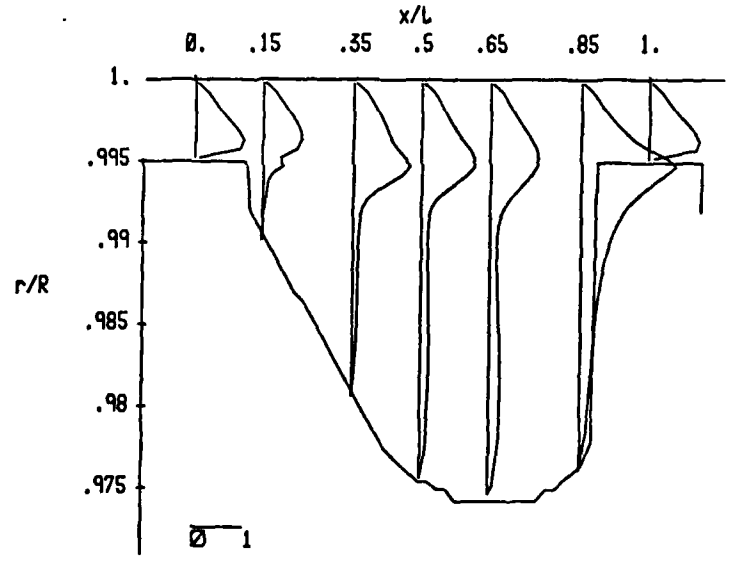

$k/U^2 \times 20$

(b) Typical cavity

Fig. 10 Predicted dimensionless turbulence kinetic energy for: (a) a generic and (b) a typical labyrinth seal cavity

END

FILMED

1-84

DTIC